Surface Interactions Surpass Carbon–Carbon Bond: Understanding and Control of the Scission Behavior of Core–Shell Polymer Brushes on Surfaces

Zhicheng Zheng,[†] Markus Müllner,[†] Jun Ling,[†,‡,*] and Axel H. E. Müller[†,*]

[†]Makromolekulare Chemie II, Universität Bayreuth, D-95440 Bayreuth, Germany and [‡]MOE Key Laboratory of Macromolecular Synthesis and Functionalization, Department of Polymer Science and Engineering, Zhejiang University, Hangzhou 310027, China. Present address: M.M. is now at the Department of Chemical & Biomolecular Engineering, University of Melbourne. A.H.E.M. is now at the Institute of Organic Chemistry, Johannes Gutenberg University, 55099 Mainz, Germany.

ABSTRACT A tapping-mode AFM investigation of core–shell cylindrical polymer brushes (CPBs) on mica shows that they can be ruptured upon spin-coating. Three different CPBs were synthesized, having a methacrylate backbone, carrying branches of poly[oligo(ethylene glycol)methacrylate] (POEGMA), POEGMA-*block*-poly[2-(dimethylamino)ethyl methacrylate] (POEGMA-*b*-PDMAEMA), and POEGMA-*block*-poly[2-(methacryloyloxy)ethyl trimethylammoniumiodide] (POEGMA-*b*-PMETAI). The polymer backbone of core–shell CPB with POEGMA-*b*-PDMAEMA or POEGMA-*b*-PMETAI branches is ruptured upon drying on a mica surface, while they are stable in aqueous solution. We propose that the scission behavior is induced by Coulomb interactions between PDMAEMA or PMETAI corona and the solid surface and that this interaction is stronger than one or more carbon–carbon single bonds. We control this scission behavior by tuning the surface interactions through switching the surface nature, varying pH, or adding multivalent counterions. Our study demonstrates that core–shell CPB serves as a template to directly compare the weak intermolecular forces with the strong carbon–carbon covalent bonds.

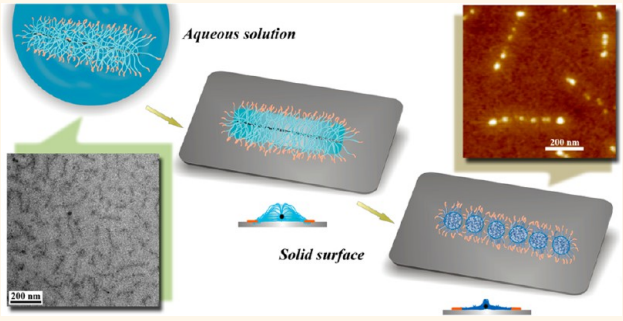

KEYWORDS: cylindrical polymer brushes · polyelectrolytes · surface charges · intermolecular attractions · surface interaction energy · carbon–carbon bond energy · scission behavior

It is an ingenious strategy to mobilize a group of many dwarves to defeat a giant. Intermolecular attraction, *the dwarf*, possesses an energy of 2–12 kJ mol^{-1}, less by 1 to 2 orders of magnitude than the carbon–carbon covalent bond, *the giant*, with an energy of 348 kJ mol^{-1}. Under some extreme conditions, the carbon–carbon covalent bond can be challenged, such as with ultrasonic field,[1] clashing flow,[2] receding interface,[3] and single molecular stretching.[4,5] Yet, in this contribution, we work out a strategy to teach hundreds and thousands of intermolecular attractions to directly combat carbon–carbon covalent bonds under ambient conditions. We employ a branched polymer architecture, that is, a core–shell cylindrical polymer brush (CPB), which consists of a single linear polymer backbone and a large number of polymer chains with functional groups in the outside shell layer.[6,7] When they cooperate to anchor on a solid surface, producing enough intermolecular attractions, and then the inner core part contracts by drying, serving as a fast responsive driving force, the carbon–carbon covalent bonds in the backbone are ruptured within minutes. The CPB residues after scission meet the situation that the remaining dwarfs are just insufficient in number to beat a giant. Therefore, the control of the extent and the position of the scission of the backbone is feasible by means of tuning the intermolecular attractions between the functional groups and the surface. Our design differs from the report of a random scission of a CPB backbone by Sheiko *et al.*,[8] where the CPB was transformed *via* very slow expansion (in hours or in days) from a three-dimensional cylindrical conformation into a two-dimensional flat one driven by a confinement-induced passive exclusion of densely grafted side chains.

* Address correspondence to lingjun@zju.edu.cn, axel.mueller@uni-mainz.de.

Received for review November 22, 2012 and accepted February 13, 2013.

Published online February 13, 2013
10.1021/nn3054347

RESULTS AND DISCUSSION

Synthesis of Cylindrical Polymer Brushes (CPBs). The "grafting from" synthetic route to different core−shell CPBs follows an established protocol[9,10] and is illustrated in Supporting Information Scheme S1. Poly[2-(2-bromoisobutyryloxy)ethyl methacrylate] (PBiEM) with the degree of polymerization, DP, of 1500 and a polydispersity index, PDI, of 1.08 was used as polyinitiator. The homopolymer CPB with poly[oligo(ethylene glycol)methacrylate] (POEGMA) side chains was prepared *via* ATRP of OEGMA from the PBiEM backbone. This well-defined CPB has an apparent PDI of 1.35. The initiating efficiency of the PBiEM polyinitiator toward OEGMA was determined as 0.50. Therefore, each CPB has 750 POEGMA side chains with a DP of 430 (short as *b*-$[O_{430}]_{750}$), as shown in Scheme 1A. A sequential grafting of the poly[2-(dimethylamino)ethyl methacrylate] (PDMAEMA) block from the homopolymer CPB *b*-$[O_{430}]_{750}$ generated the core−shell CPB with diblock copolymer side chains of POEGMA-*b*-PDMAEMA (short as *b*-$[O_{430}D_{40}]_{750}$, shown in Scheme 1B,D). The core−shell CPB *b*-$[O_{430}D_{40}]_{750}$ is also well-defined and has an apparent PDI of 1.28. The DP of the PDMAEMA block was determined as 40, and thus the weight fraction (wt %) of PDMAEMA segments in the CPB *b*-$[O_{430}D_{40}]_{750}$ is only 4.6%. Quaternization of the PDMAEMA block with iodomethane led to core−shell CPBs with a POEGMA core and a polyelectrolyte shell of poly[2-(methacryloyloxy)-ethyl trimethylammoniumiodide] (PMETAI) (short as *b*-$[O_{430}Dq_{40}]_{750}$, shown in Scheme 1C). The characterization of different CPBs by proton nuclear magnetic resonance (^{1}H NMR) and size exclusion chromatography (SEC) is given in Figures S1 and S2.

Scission of CPBs on Mica Surface. After being spin-coated onto the mica surface from dilute aqueous solution (pH 5.5), tapping-mode AFM images of the core−shell CPB *b*-$[O_{430}D_{40}]_{750}$ showed a completely different conformation than that of the homopolymer CPB *b*-$[O_{430}]_{750}$, even though the fraction of PDMAEMA segments is very low (4.6%) (Figures 1A−F and S3A−C). In the core part of CPB *b*-$[O_{430}D_{40}]_{750}$ with the number-average length L_n = 261 ± 21 nm, mainly five or six separated small beads with a width of *ca.* 50 nm are observed. The cross-sectional analysis shows obvious gaps (up to 30 nm in width) between two adjacent beads, which reach the surface basis, as shown in Figure 1F. In contrast, the homopolymer CPB *b*-$[O_{430}]_{750}$ has a homogeneous and continuous conformation with L_n = 172 ± 20 nm and a width of *ca.* 70 nm (Figure 1A−C) on the mica surface. In the case of CPB *b*-$[O_{430}Dq_{40}]_{750}$, which carries quaternized PDMAEMA segments in the periphery, a noncontinuous conformation is observed with even more small beads (mainly 9 or 10) with a width of *ca.* 45 nm in the core part, as shown in Figures 1G−I and S3D−F. The average length, L_n, of the CPB *b*-$[O_{430}Dq_{40}]_{750}$ was measured as 376 ± 25 nm, which equals the contour length (375 nm) of the PBiEM backbone with a DP of 1500. This noncontinuous and fully stretched conformation as well as the obvious gaps between adjacent beads indicates that the core−shell CPBs had ruptured.

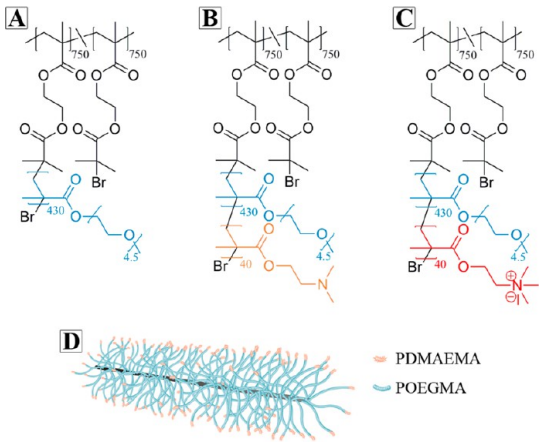

Scheme 1. Chemical structures of the homopolymer CPB *b*-$[O_{430}]_{750}$ (A), the core−shell CPB *b*-$[O_{430}D_{40}]_{750}$ (B), and the core−shell CPB *b*-$[O_{430}Dq_{40}]_{750}$ (C). Schematic illustration of the core−shell CPB *b*-$[O_{430}D_{40}]_{750}$ (D).

CPBs in Aqueous Solution. To prove that the scission of core−shell CPBs happens only after spin-coating onto surfaces rather than in the previous aqueous solution, aqueous solution (pH 5.5) of different CPBs was characterized by dynamic light scattering (DLS) and cryogenic transmission electron microscopy (cryo-TEM). Although DLS measurements only give an apparent dimension for wormlike CPBs, the apparent hydrodynamic radius, $R_{h,app}$, reflects the overall changes of CPBs in aqueous solution.[11] The monomodal and narrow $R_{h,app}$ distributions of different CPBs (Figure 2A) indicate that the CPBs were well-dissolved and stayed stable in aqueous solution without detectable constitution changes. Furthermore, only continuous wormlike conformations observed for both CPBs *b*-$[O_{430}D_{40}]_{750}$ and *b*-$[O_{430}Dq_{40}]_{750}$ in cryo-TEM (Figure 2B,C) directly confirm that the core−shell CPBs were not ruptured in aqueous solution. The L_n values of CPBs *b*-$[O_{430}D_{40}]_{750}$ and *b*-$[O_{430}Dq_{40}]_{750}$ are underestimated in the measurement as 172 and 265 nm, respectively, since wormlike CPBs stay tilted in the specimen film with a thickness of *ca.* 200 nm for cryo-TEM and only the projection is measured. Assuming an average tilting angle of 40°, L_n values of CPBs *b*-$[O_{430}D_{40}]_{750}$ and *b*-$[O_{430}Dq_{40}]_{750}$ are corrected to 226 and 348 nm, respectively, and they are in good agreement with the dimensions measured from AFM images (Figures 1 and S3). In addition, a sample of the CPB *b*-$[O_{430}Dq_{40}]_{750}$ was prepared by applying its aqueous solution onto mica, which was then kept in water for contact-mode AFM in liquid. The height image also shows a continuous wormlike conformation (Figure S4), indicating that the CPB is stable even after being adsorbed on mica as long as it is not dried. The scission behavior observed in

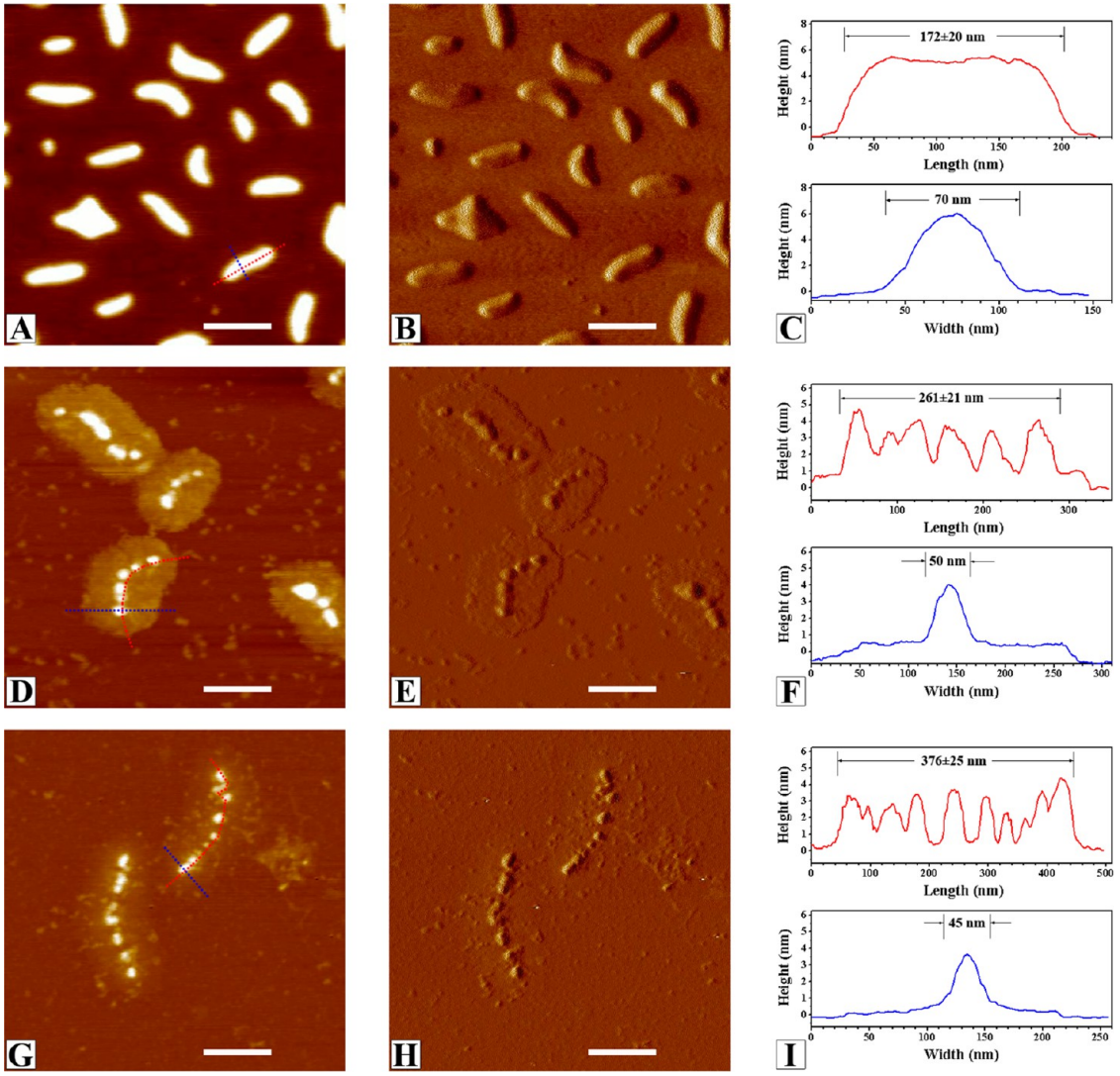

Figure 1. Tapping-mode AFM height image, phase image, and the corresponding height cross-section analysis of CPBs *b*-$[O_{430}]_{750}$ (A–C), *b*-$[O_{430}D_{40}]_{750}$ (D–F), and *b*-$[O_{430}Dq_{40}]_{750}$ (G–I). CPBs were spin-coated on a freshly cleaved mica surface from 0.02 g L^{-1} aqueous solution (pH 5.5). The *Z*-ranges are 8 nm for height images and 10° for phase images. The scale bars correspond to 200 nm.

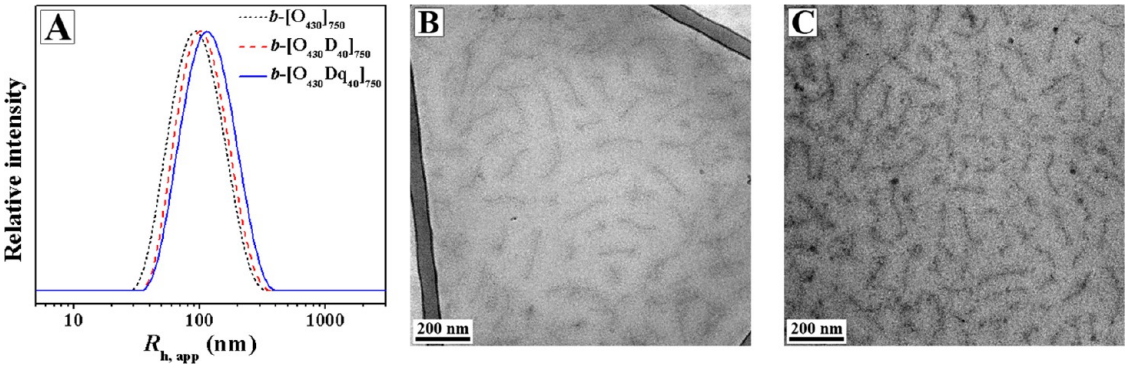

Figure 2. Intensity-weighted DLS CONTIN plots for CPBs in 0.2 g L^{-1} aqueous solution (pH 5.5) (A), $\langle R_{h,app}\rangle_z$ = 92, 102, and 112 nm, PDI = 1.16, 1.15, and 1.16 for *b*-$[O_{430}]_{750}$ (black), *b*-$[O_{430}D_{40}]_{750}$ (red), and *b*-$[O_{430}Dq_{40}]_{750}$ (blue), respectively. Cryo-TEM images of CPBs *b*-$[O_{430}D_{40}]_{750}$ (B) and *b*-$[O_{430}Dq_{40}]_{750}$ (C) in 0.24 g L^{-1} aqueous solution (pH 5.5), $L_n = 172 \pm 23$ and 265 ± 38 nm for *b*-$[O_{430}D_{40}]_{750}$ and *b*-$[O_{430}Dq_{40}]_{750}$, respectively.

Figure 1 thus is related to the drying process during spin-coating.

Understanding the Scission Behavior of CPB *b*-$[O_{430}D_{40}]_{750}$ on Mica. On the basis of the above experimental results,

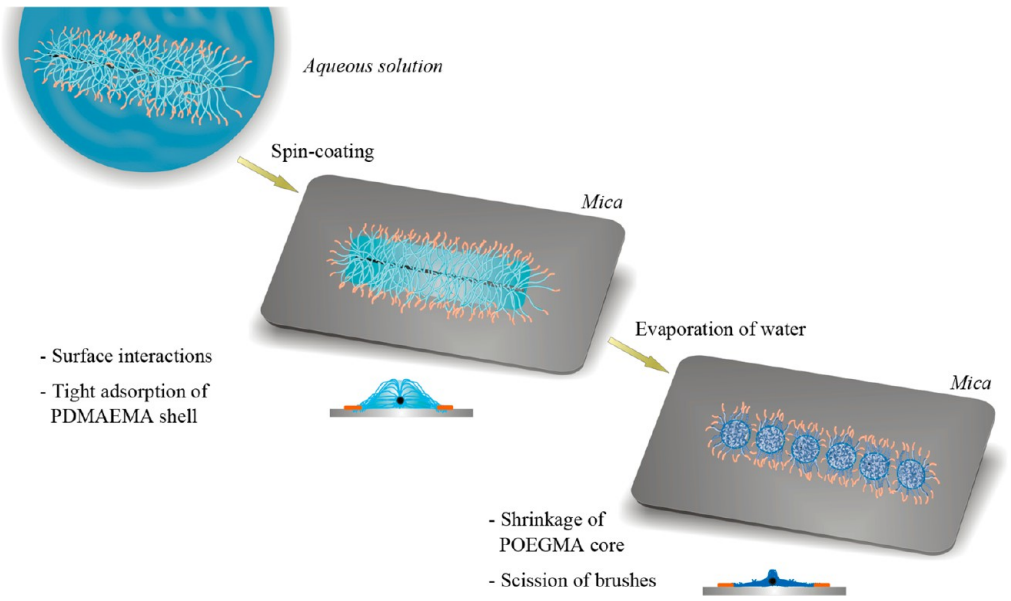

Figure 3. Illustration of scission behavior of the core−shell CPB *b*-$[O_{430}D_{40}]_{750}$ on the mica surface.

we propose a scission mechanism of the core−shell CPB *b*-$[O_{430}D_{40}]_{750}$ on mica surface as illustrated in Figure 3. In aqueous solution, the well-dissolved CPB extends side chains in all directions. Upon the instant contact of the CPB with the mica surface during spin-coating, the PDMAEMA segments tightly anchor to mica as telechelic claws due to the Coulombic interactions between the tertiary amino groups and the negatively charged mica surface (2×10^6 negative charges/μm^2),[12,13] whereas the POEGMA segments of the core carry water molecules within their ethylene ether units.[14] Subsequently, the water molecules begin to evaporate from the CPB, resulting in a contraction of the POEGMA core, both along and perpendicular to the backbone. Hence, in order to fulfill the volume change during the drying-induced shrinking process, either the PDMAEMA−mica interactions or the carbon−carbon covalent single bonds of the backbone have to be destroyed. If the energy of interactions between PDMAEMA segments and the mica surface, $E_{D,S}$, are n times as strong as that of a carbon−carbon covalent single bond, E_{CB}, n carbon−carbon covalent single bonds will break and the CPB will be ruptured into $n + 1$ small beads. We found that the CPB *b*-$[O_{430}D_{40}]_{750}$ was ruptured into mainly five or six small beads in the core part (Figures 1D−F and S3A−C) after being spin-coated onto mica, which indicates that the energy of the combined surface interactions, $E_{D,S}$, is in the range of 4 to 5 times that of the carbon−carbon covalent single bond energy, E_{CB}. The dependence of the number of small beads, N_{beads}, in the ruptured CPB on the energy of combined surface interactions, E_{SI}, can be described by eq 1:

$$N_{beads} - 1 = \frac{E_{SI}}{E_{CB}} = \frac{\sum_i E_{P,i}}{E_{CB}} = \frac{\sum_i \left(- \int \boldsymbol{F}_i \cdot d\boldsymbol{S}_i \right)}{E_{CB}} \quad (1)$$

where $E_{P,i}$, F_i, and dS_i are the PDMAEMA−substrate attractive potential energy of a single DMAEMA unit, the corresponding intermolecular attractive force, and differential replacement, respectively. In the case of CPB *b*-$[O_{430}Dq_{40}]_{750}$ carrying polyelectrolyte PMETAI segments, the intermolecular attraction, $F_{Dq,S}$, is higher than that of PDMAEMA, $F_{D,S}$, since the densely positively charged PMETAI segments have stronger electrostatic interactions with the negative charges on mica.[15] Assuming that the number of METAI units which contact the mica surface in CPB *b*-$[O_{430}Dq_{40}]_{750}$ is the same as that of DMAEMA units in the precursor CPB *b*-$[O_{430}D_{40}]_{750}$, eq 1 predicts that CPB *b*-$[O_{430}Dq_{40}]_{750}$ should be ruptured into more small beads on mica than the CPB *b*-$[O_{430}D_{40}]_{750}$. This is confirmed by the observation of mainly 9 or 10 small beads in the AFM images (Figures 1G−I and S3D−F). Therefore, the above theory can be applied to control the scission behavior of core−shell CPBs on surfaces by tuning the intermolecular attraction, F, and thus the surface interaction energy.

Scission of CPBs on Silicon Surface. An alternate way to tune the intermolecular attraction, F, is to change nature of the surface. The surface of silicon is very slightly charged at pH 5.5,[16] providing weaker attraction than mica with either PDMAEMA or PMETAI segments, that is, $F_{D,Si} < F_{D,mica}$ and $F_{Dq,Si} < F_{Dq,mica}$. As shown in Figures 4A−C and S5A,B, in contrast to the scission conformation on mica (Figure 1D−F), the CPB *b*-$[O_{430}D_{40}]_{750}$ shows a "fried egg"-like conformation with a continuous homogeneous core on silicon (Figure 4D−F). The core of CPB *b*-$[O_{430}D_{40}]_{750}$ was measured as 134 and 9 nm in length and height, respectively, which is shorter but higher than that on mica (261 and 4 nm). This conformation of CPB *b*-$[O_{430}D_{40}]_{750}$ is explained by the weaker interaction energy. During the drying-induced volume contraction

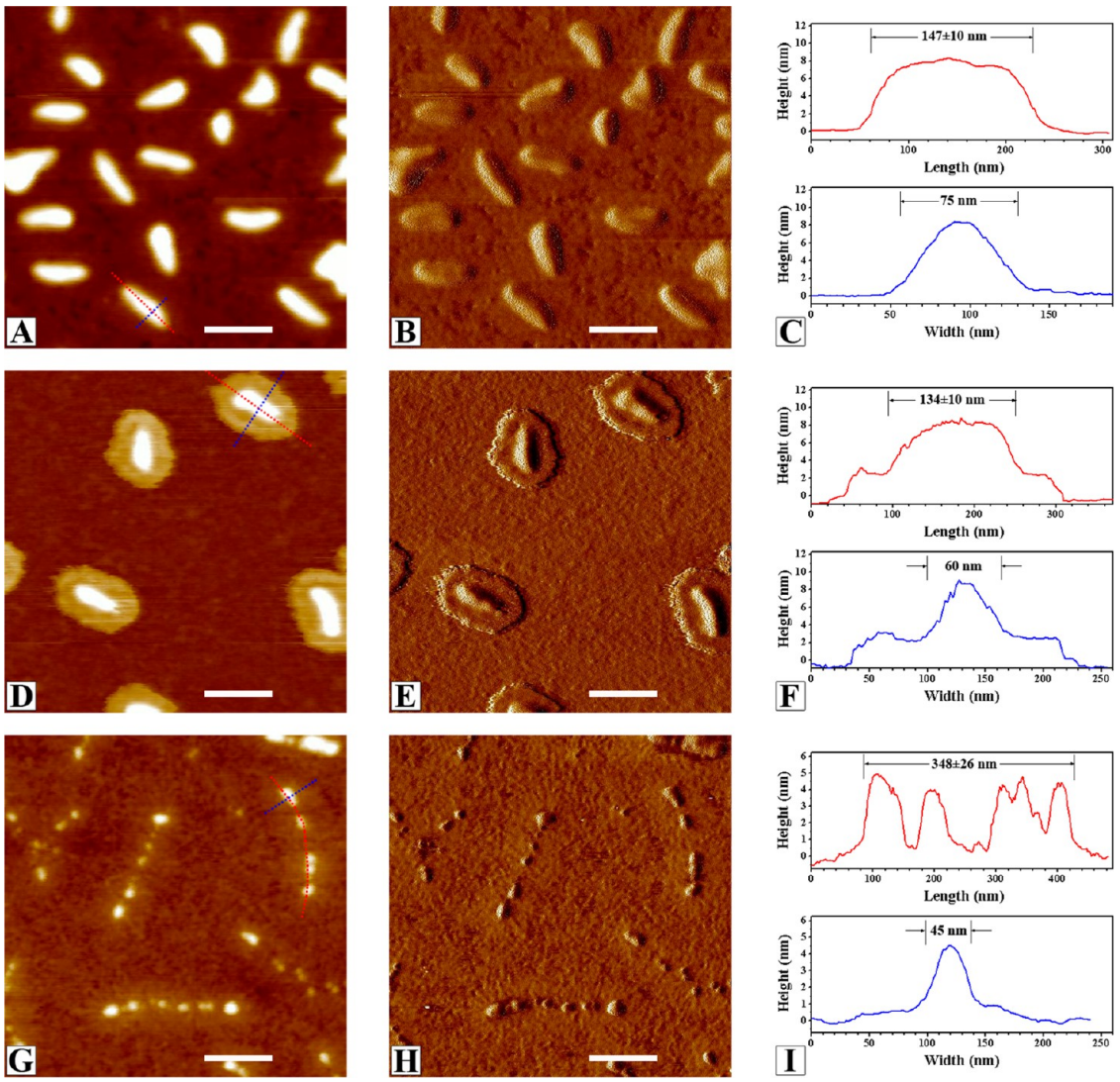

Figure 4. Tapping-mode AFM height image, phase image, and the corresponding height cross-section analysis of CPBs *b*-$[O_{430}]_{750}$ (A–C), *b*-$[O_{430}D_{40}]_{750}$ (D–F), and *b*-$[O_{430}Dq_{40}]_{750}$ (G–I). CPBs were spin-coated on the silicon surface from 0.02 g L^{-1} aqueous solution (pH 5.5). The *Z*-ranges are 12 nm for height images and 10° for phase images. The scale bars correspond to 200 nm.

process of the POEGMA core, the PDMAEMA telechelic claws are sliding rather than anchoring on the silicon surface, leading to a shorter but more compact and continuous core part in the final conformation. Taking CPB *b*-$[O_{430}Dq_{40}]_{750}$ carrying strongly positively charged PMETAI segments on silicon into account, $F_{Dq,Si} > F_{D,Si}$ but $F_{Dq,Si} < F_{Dq,mica}$, leading to a noncontinuous conformation with mainly five or six small beads in the core part, as observed in Figures 4G–I and S5C–E. Therefore, the energy of surface interactions between PMETAI segments and silicon, $E_{Dq,Si}$, is in the range of 4 to 5 times that of the carbon–carbon covalent single bond energy, E_{CB}.

pH Value as a Trigger To Control the Scission of the CPB *b*-$[O_{430}D_{40}]_{750}$ on Mica. The pH-dependent protonation degree of the PDMAEMA segments of the CPB *b*-$[O_{430}D_{40}]_{750}$ affects the intermolecular attraction, *F*, between the outside shell layer and the negatively charged mica surface. On the basis of eq 1, tuning the pH value of the aqueous solution of CPB *b*-$[O_{430}D_{40}]_{750}$ is a way to control its scission behavior. For instance, elevated PDMAEMA protonation at low pH increases surface interactions, $E_{D,S}$, between PDMAEMA segments and mica and thus should increase the number of small beads, N_{beads}, in the ruptured CPB. The samples in Figures 1 and 4 were prepared from aqueous solutions at pH 5.5, resulting in a *ca.* 50% protonation of the CPB *b*-$[O_{430}D_{40}]_{750}$ (the star polymer $(PDMAEMA_{240})_{24}$ has $pK_a = 5.8$[17]). Two samples of CPB *b*-$[O_{430}D_{40}]_{750}$ were prepared from 0.02 g L^{-1} aqueous solutions at pH 1.9 and 10.0, where the PDMAEMA segments are fully protonated and fully deprotonated, respectively. In the case of pH 1.9, the core part was ruptured into mainly six or seven small beads (Figures 5A–C and S6A–C), more than that at pH 5.5 (Figure 1D–F). In contrast, upon increasing the pH to 10.0, only three or four beads were observed in the core part of CPB (Figures 5D–F and S6D–F).

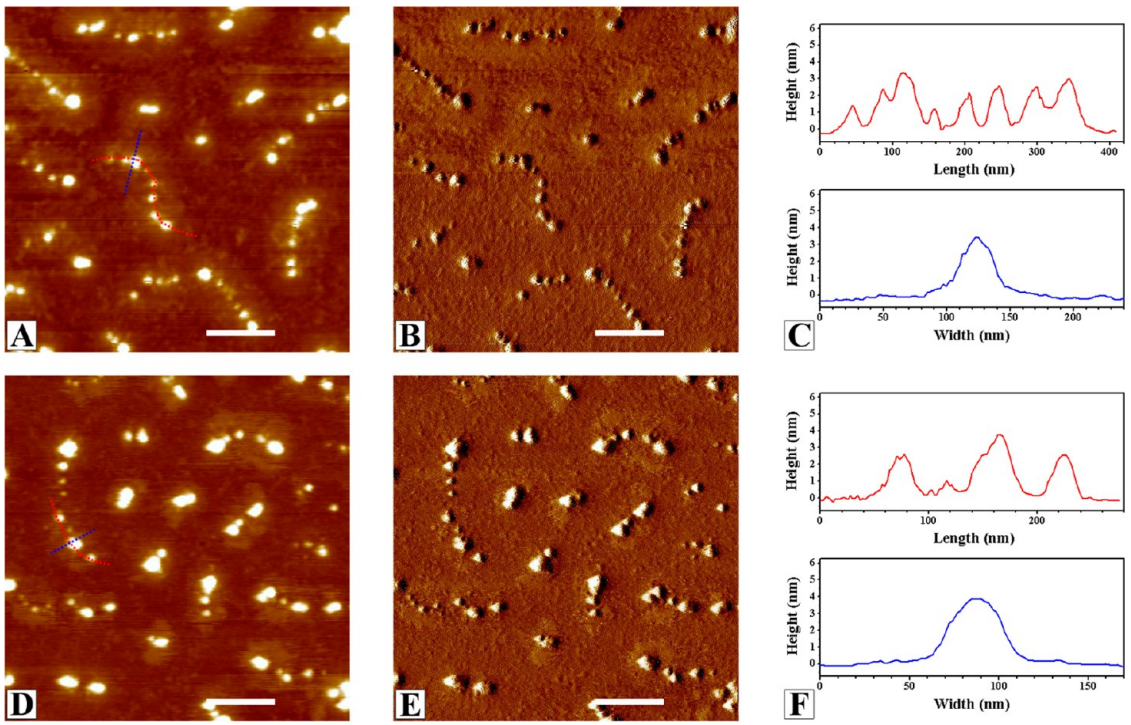

Figure 5. Tapping-mode AFM height image, phase image, and the corresponding height cross-section analysis of the CPB *b*-$[O_{430}D_{40}]_{750}$ spin-coated on mica surface from 0.02 g L^{-1} aqueous solution at pH 1.9 (A–C) and at pH 10.0 (D–F). The *Z*-ranges are 8 nm for height images and 10° for phase images. The scale bars correspond to 200 nm.

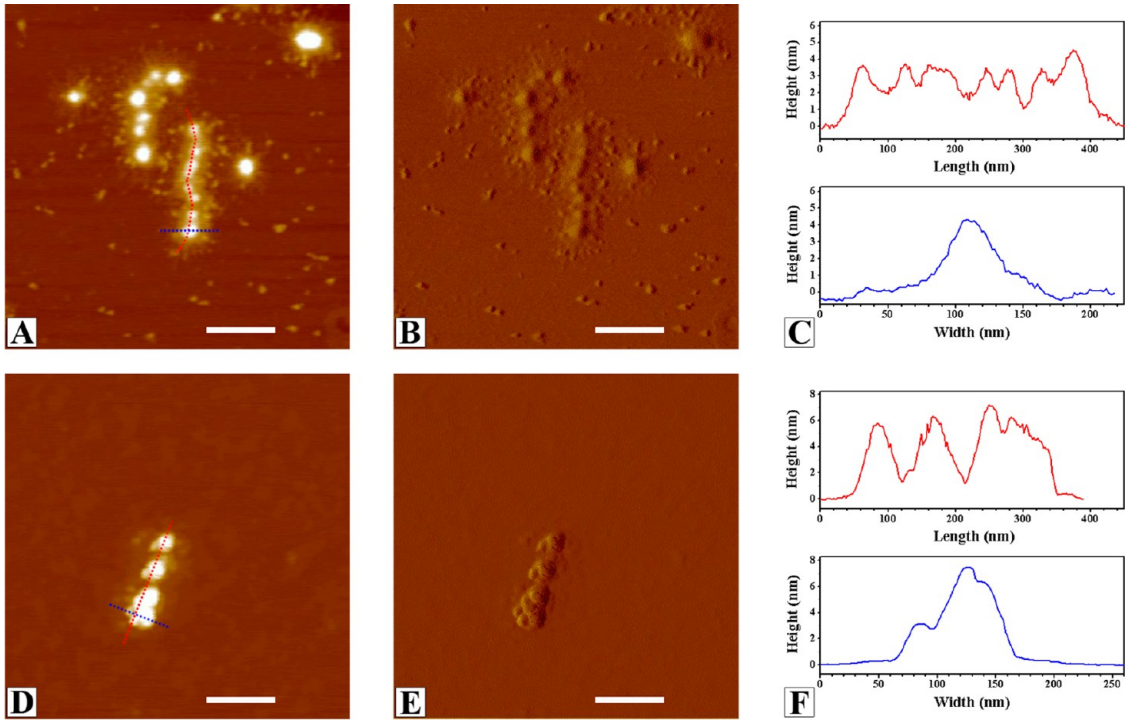

Figure 6. Tapping-mode AFM height image, phase image, and the corresponding height cross-section analysis of CPBs *b*-$[O_{430}Dq_{40}]_{750}$ (0.02 g L^{-1} aqueous solution, pH 5.5) containing 3.9 μM of $K_3[Co(CN)_6]$ (A–C) and 7.8 μM of $K_3[Co(CN)_6]$ (D–F). CPBs were spin-coated on freshly cleaved mica surface. The *Z*-ranges are 8 nm for height images and 10° for phase images. The scale bars correspond to 200 nm.

Multivalent Counterion as a Trigger To Control the Scission of CPB *b*-$[O_{430}Dq_{40}]_{750}$. Homopolymer CPBs with PMETAI side chains conformationally respond to multivalent counterions in aqueous solution as reported in our previous work.[11] Exchanging some monovalent iodide counterions of the PMETAI segments by multivalent

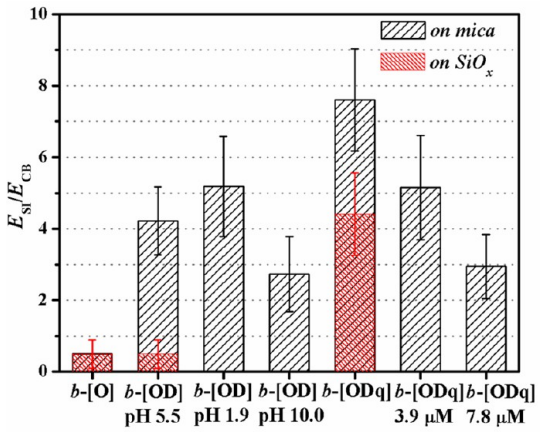

Figure 7. Comparison of combined surface interaction energy, E_{SI}, of different CPBs on various surfaces (mica, black; silicon, red) relative to the carbon−carbon covalent bond energy, E_{CB}. The last two samples contain the given concentration of $[Co(CN)_6]^{3-}$ ions.

counterions decreases the osmotic pressure within the brush, screening the electrostatic interactions between the positively charged telechelic segments of the CPB b-$[O_{430}Dq_{40}]_{750}$ and the negative charges on mica. Accordingly, intermolecular attraction, F, should decrease. As indicated in eq 1, the core part of CPB is expected to be ruptured into fewer small beads on mica. To confirm this, we prepared 0.02 g L^{-1} aqueous solutions (pH 5.5) of the CPB b-$[O_{430}Dq_{40}]_{750}$, (containing 5.7 μM iodide ions) and added $K_3[Co(CN)_6]$ to reach 3.9 and 7.8 μM concentrations of $[Co(CN)_6]^{3-}$ ions, respectively. As predicted, the core part of CPB was ruptured into mainly six or seven small beads as observed in the tapping-mode AFM images of b-$[O_{430}Dq_{40}]_{750}$ containing 3.9 μM of $K_3[Co(CN)_6]$ on mica (Figures 6A−C and S7A−C). In the sample containing 7.8 μM of $K_3[Co(CN)_6]$, the core part of CPB was broken into even fewer small beads (three or four) on mica (Figures 6D−F and S7D−F), as intermolecular attraction, F, between the telechelic segments and mica is lower than that with 3.9 μM salt.

Comparison of Surface Interaction Energies of Different CPBs. By employing eq 1, we estimate the ratio of combined surface interaction energy, E_{SI}, of CPBs to the carbon−carbon covalent single bond energy, E_{CB}, from the number of small beads, N_{beads}, in the core part. According to the statistic results (Figures 1, 4−6, S3, and S5−S7), we summarize the ratio $E_{SI}/E_{CB} = N_{beads} - 1$ of different CPBs on surfaces in Figure 7. For the homopolymer CPB b-$[O_{430}]_{750}$, the surface interaction energy, E_{SI}, is lower than the carbon−carbon covalent bond energy, E_{CB}, on both mica and silicon, where the CPB is not ruptured. In all cases of core−shell CPBs on surfaces, except b-$[O_{430}D_{40}]_{750}$ on silicon, the surface interactions surpass the carbon−carbon covalent bond, that is, the ratio $E_{SI}/E_{CB} > 1$, resulting in the scission of CPBs on surfaces. Compared to the CPB b-$[O_{430}D_{40}]_{750}$, the CPB b-$[O_{430}Dq_{40}]_{750}$ with a high density of positive charges in polyelectrolyte PMETAI segments shows stronger surface interactions on both mica and silicon. However, silicon as a nearly neutral surface gives weaker interactions than mica with either PDMAEMA or PMETAI segments. The surface interactions between PDMAEMA segments and mica increase with decreasing pH values (*i.e.*, increasing protonation). Adding multivalent counterions into the aqueous solution of the CPB b-$[O_{430}Dq_{40}]_{750}$ reduces the electrostatic interactions between the positively charged PMETAI segments and the negative charges on mica, thus decreasing the ratio E_{SI}/E_{CB}.

CONCLUSIONS

The polymer backbone of core−shell CPB is ruptured upon drying under ambient conditions when the functional groups in the outside shell produce enough intermolecular interactions with a solid surface. We successfully tune the surface interactions to control this scission behavior of different core−shell CPBs by means of switching the surface nature, quaternization, varying the pH value, or adding multivalent counterions. Our study demonstrates that core−shell CPB as a branched polymer architecture provides a platform for a direct dialogue between the weak intermolecular forces and the strong carbon−carbon covalent bonds.

EXPERIMENTAL SECTION

Preparation of CPBs. The synthesis of the polyinitiator poly-[2-(2-bromoisobutyryloxy)ethyl methacrylate] (PBiEM) (DP_n = 1500, PDI = 1.08) by anionic polymerization, acidic cleavage of the trimethylsilyl groups, and an esterification to attach the ATRP initiating sites was reported previously.[18] The homopolymer CPB b-$[O_{430}]_{750}$ was synthesized *via* ATRP from the PBiEM backbone. A flask equipped with CuBr and polyinitiator PBiEM was degassed with argon for 30 min. Then degassed monomer OEGMA and solvent anisole were added by syringe. The mixture was stirred and heated to 60 °C. Finally, the degassed ligand, *N*,*N*,*N*′,*N*″,*N*″-pentamethyldiethylenetriamine (PMDETA), was injected to start the polymerization, and an initial sample was taken for ^{1}H NMR measurement. The polymerization was monitored by withdrawing samples for ^{1}H NMR measurements. When a desired conversion was achieved, the reaction was quenched by cooling the reaction mixture to room temperature and exposing it to air. The reaction mixture was purified by passing through a silica gel column, followed by precipitating into cold *n*-hexane.

The core−shell CPB b-$[O_{430}D_{40}]_{750}$ was obtained *via* ATRP of DMAEMA from the homopolymer CPB b-$[O_{430}]_{750}$. A round-bottom flask was charged with CuBr, b-$[O_{430}]_{750}$, and anisole. The mixture was degassed with argon for 30 min. After that, the degassed monomer DMAEMA was added by syringe into the flask, which was then heated to 90 °C. The degassed ligand PMDETA was injected to start the polymerization. As described above, the polymerization was monitored by ^{1}H NMR measurements. After achieving a desired conversion, the reaction was quenched by cooling the reaction mixture to room temperature and exposing it to air. The reaction mixture was purified by passing through a silica gel column, followed by precipitating into cold *n*-hexane twice.

The core−shell CPB b-$[O_{430}Dq_{40}]_{750}$ carrying polyelectrolyte PMETAI segments was synthesized *via* quaternization of the PDMAEMA segments of the CPB b-$[O_{430}D_{40}]_{750}$. Here, b-$[O_{430}D_{40}]_{750}$ was dissolved in dioxane (about 10 mg/mL). Methyl iodide was added at room temperature at a molar ratio of 2 compared to amino groups. After around 20 min, the solution became turbid. Stirring was continued for 2 days to ensure the full reaction. Then the turbid reaction mixture was transferred into a dialysis membrane and dialyzed against pure water for 1 week.

Determination of the Initiating Efficiency. The initiating efficiency of the polyinitiator PBiEM toward OEGMA was determined by cleaving POEGMA side chains from the CPB b-$[O_{430}]_{750}$ under alkaline conditions. The obtained PMAA linear polymers were methylated into PMMA, which was characterized by SEC. The procedure was detailed in our earlier work.[19]

Characterization Methods. *Size Exclusion Chromatography.* SEC was conducted using dimethyl acetamide (DMAc) with 0.05% lithium bromide as eluent at an elution rate of 0.8 mL/min. The equipment consists of one precolumn and two analytical columns (PSS GRAM, 10^2 and 10^3 Å pore size, 7 mm particle size) and an Agilent 1200 RI detector. The measurements were performed at 60 °C. PDMAEMA calibration curve was used to calibrate the columns.

^{1}H Nuclear Magnetic Resonance Spectroscopy. ^{1}H NMR measurements were carried out on a Bruker AC-300 instrument at room temperature in $CDCl_3$ or D_2O.

Tapping-Mode Atomic Force Microscopy. AFM images were recorded on a Digital Instruments Dimension 3100 microscope operated in tapping mode. The samples were prepared by spin-coating (3000 rpm, 1 min) diluted aqueous solutions onto mica or silicon surface.

Contact-Mode Atomic Force Microscopy in Liquid. AFM images were recorded on a JPK Nanowizard I equipment. The sample was prepared by dipping diluted aqueous solution onto mica which was glued on a glass dish containing Milli-Q pure water.

Conflict of Interest: The authors declare no competing financial interest.

Acknowledgment. Z.Z. appreciates a scholarship from the Elite Support Program of Bavaria. J.L. sincerely thanks the Alexander von Humboldt Foundation for granting him a research fellowship. We thank Melanie Förtsch for cryo-TEM measurements and Dr. Oleg Borisov for helpful discussions.

Supporting Information Available: Synthetic route, ^{1}H NMR spectra, SEC profiles, AFM images with larger scan sizes, and histograms. This material is available free of charge *via* the Internet at http://pubs.acs.org.

REFERENCES AND NOTES

1. Basedow, A. M.; Ebert, K. H. Ultrasonic Degradation of Polymer in Solution. *Adv. Polym. Sci.* **1977**, *22*, 83–148.
2. Odell, J. A.; Keller, A.; Rabin, Y. Flow-Induced Scission of Isolated Macromolecules. *J. Chem. Phys.* **1988**, *88*, 4022–4028.
3. Bensimon, A.; Simon, A.; Chiffaudel, A.; Croquette, V.; Heslot, F.; Bensimon, D. Alignment and Sensitive Detection of DNA by a Moving Interface. *Science* **1994**, *265*, 2096–2098.
4. Kishino, A.; Yanagida, T. Force Measurements by Micromanipulation of a Single Actin Hilament by Glass Needles. *Nature* **1988**, *334*, 74–76.
5. Mehta, A. D.; Rief, M.; Spudich, J. A.; Smith, D. A.; Simmons, R. M. Single-Molecule Biomechanics with Optical Methods. *Science* **1999**, *283*, 1689–1695.
6. Zhang, M.; Müller, A. H. E. Cylindrical Polymer Brushes. *J. Polym. Sci., Part A: Polym. Chem.* **2005**, *43*, 3461–3481.
7. Sheiko, S. S.; Sumerlin, B. S.; Matyjaszewski, K. Cylindrical Molecular Brushes: Synthesis, Characterization, and Properties. *Prog. Polym. Sci.* **2008**, *33*, 759–785.
8. Sheiko, S. S.; Sun, F. C.; Randall, A.; Shirvanyants, D.; Rubinstein, M.; Lee, H.; Matyjaszewski, K. Adsorption-Induced Scission of Carbon−Carbon Bonds. *Nature* **2006**, *440*, 191–194.
9. Yuan, J.; Xu, Y.; Walther, A.; Bolisetty, S.; Schumacher, M.; Schmalz, H.; Ballauff, M.; Müller, A. H. E. Water-Soluble Organo-Silica Hybrid Nanowires. *Nat. Mater.* **2008**, *7*, 718–722.
10. Müllner, M.; Yuan, J.; Weiss, S.; Walther, A.; Förtsch, M.; Drechsler, M.; Müller, A. H. E. Water-Soluble Organo-Silica Hybrid Nanotubes Templated by Cylindrical Polymer Brushes. *J. Am. Chem. Soc.* **2010**, *132*, 16587–16592.
11. Xu, Y.; Bolisetty, S.; Drechsler, M.; Fang, B.; Yuan, J.; Harnau, L.; Ballauff, M.; Müller, A. H. E. Manipulating Cylindrical Polyelectrolyte Brushes on the Nanoscale by Counterions: Collapse Transition to Helical Structures. *Soft Matter* **2009**, *5*, 379–384.
12. Güven, N. Crystal-Structures of 2M1 Phengite and 2M1 Muscovite. *Z. Kristallogr.* **1971**, *134*, 196–212.
13. Rojas, O. J.; Ernstsson, M.; Neuman, R. D.; Claesson, P. M. Effect of Polyelectrolyte Charge Density on the Adsorption and Desorption Behavior on Mica. *Langmuir* **2002**, *18*, 1604–1612.
14. Keefe, A. J.; Jiang, S. Poly(zwitterionic) Protein Conjugates Offer Increased Stability without Sacrificing Binding Affinity or Bioactivity. *Nat. Chem.* **2012**, *4*, 59–63.
15. Dahlgren, M. A. G.; Claesson, P. M.; Audebert, R. Highly Charged Cationic Polyelectrolytes on Mica: Influence of Polyelectrolyte Concentration on Surface Forces. *J. Colloid Interface Sci.* **1994**, *166*, 343–349.
16. Buron, C. C.; Filiâtre, C.; Membrey, F.; Bainier, C.; Charraut, D.; Foissy, A. Early Steps in Layer-by-Layer Construction of Polyelectrolyte Flms: The Transition from Surface/Polymer to Polymer/Polymer Determining Interactions. *J. Colloid Interface Sci.* **2007**, *314*, 358–366.
17. Plamper, F. A.; Ruppel, M.; Schmalz, A.; Borisov, O.; Ballauff, M.; Müller, A. H. E. Tuning the Thermoresponsive Properties of Weak Polyelectrolytes: Aqueous Solutions of Star-Shaped and Linear Poly(*N*,*N*-dimethylaminoethyl methacrylate). *Macromolecules* **2007**, *40*, 8361–8366.
18. Zhang, M.; Breiner, T.; Mori, H.; Müller, A. H. E. Amphiphilic Cylindrical Brushes with Poly(acrylic acid) Core and Poly(*n*-butyl acrylate) Shell and Narrow Length Distribution. *Polymer* **2003**, *44*, 1449–1458.
19. Plamper, F. A.; Schmalz, A.; Penott-Chang, E.; Drechsler, M.; Jusufi, A.; Ballauff, M.; Müller, A. H. E. Synthesis and Characterization of Star-Shaped Poly(*N*,*N*-dimethylaminoethyl methacrylate) and Its Quaternized Ammonium Salts. *Macromolecules* **2007**, *40*, 5689–5697.